International Journal of Mass Spectrometry 274 (2008) 14–20

Contents lists available at ScienceDirect

International Journal of Mass Spectrometry

journal homepage: www.elsevier.com/locate/ijms

Electron impact ionization and ion–molecule reactions of octafluoro-2-butene

C.Q. Jiao[a], C.A. DeJoseph Jr.[b], R. Lee[b], A. Garscadden[b,*]

[a] Innovative Scientific Solutions, Inc., Dayton, OH 45440-3638 USA
[b] Air Force Research Laboratory, Wright-Patterson AFB, OH 45433-7251 USA

ARTICLE INFO

Article history:
Received 11 January 2008
Received in revised form 3 April 2008
Accepted 10 April 2008
Available online 18 April 2008

Keywords:
Dissociative ionization
Ion–molecule
2-C4F8
Cross-section

ABSTRACT

Electron impact ionization and ion–molecule reactions of octafluoro-2-butene (*2*-C_4F_8) were studied using Fourier transform mass spectrometry (FTMS). Fifteen product ions are formed by electron impact ionization over the energy range 10–200 eV, with $C_4F_{7,8}^+$, $C_3F_{3,5,6}^+$, $C_2F_4^+$ and CF_{1-3}^+ as the major ions. The total ionization cross-section reaches a maximum of 1.2×10^{-15} cm^2 at 90 eV. From threshold to 18 eV, the ion population is dominated by the parent ion $C_4F_8^+$, and from 18 to 70 eV, by $C_3F_5^+$. Above 70 eV, CF_3^+ becomes the dominant ion. Among the major ions formed by electron impact ionization of *2*-C_4F_8, only CF^+, CF_2^+ and CF_3^+ are found to react with the parent molecule, via F^- transfer or charge transfer mechanisms. The charge transfer reaction of Ar^+ with *2*-C_4F_8 produces mainly $C_4F_7^+$. The ion chemistries in *2*-C_4F_8 are significantly different from those in *c*-C_4F_8 that we have previously studied.

Published by Elsevier B.V.

1. Introduction

In the semiconductor industry, saturated perfluorocarbons (PFCs) such as CF_4, C_2F_6, C_3F_8, and *c*-C_4F_8 have been widely used as dry-etch gases for dielectric etch. *c*-C_4F_8 in particular has been extensively used, in part because its relatively high C/F ratio, compared to the other PFCs, facilitates the formation of a C:F film on Si or SiN, which acts as an etching barrier to improve the selectivity [1]. PFCs are not environmentally friendly gases, however, because they have long atmospheric lifetimes and are extremely strong absorbers of infrared radiation, which result in high global warming potentials. Several classes of alternative candidates for PFCs have been proposed and evaluated, including hydrofluorocarbons (HFCs) [2–5], iodofluorocarbons (IFCs) [3,6–8], and unsaturated fluorocarbons (UFCs) [1,8–12]. UFCs are considered to be good replacement gases because they readily decompose in the atmosphere, through their reactions with hydroxyl radicals via the double bond, and because they have good etch properties since the double bond is selectively broken leading to a relatively stable cracking pattern for radicals and ions [12]. Recently several UFCs including hexafluoropropene (C_3F_6), hexafluorobutadiene (C_4F_6), octafluoro-2-butene (*2*-C_4F_8), octatfluoropentadiene (C_5F_8), etc., have been studied for their etch performance in comparison to the conventional etching gases such as *c*-C_4F_8 [1,11,12]. In one study [12] it was found that among the etching gases C_3F_6, C_4F_6, *c*-C_4F_8, *2*-C_4F_8 and C_5F_8, the *2*-C_4F_8 plasma exhibited the greatest etching efficiency. It was suggested that this resulted from a higher plasma density, and a higher CF_3^+/CF^+ ratio which, due to a greater etching ability of CF_3^+ compared to CF^+, can be used as an indicator of etching efficiency [12].

Given the central role played by ion bombardment in these plasma etching processes [12], it is important to acquire the kinetic data for the formation and reactions of ions in the fluorocarbon compounds. Previously we have reported ion chemistries in *c*-C_4F_8 [13]. For comparison, in this paper we present our recent measurements on the electron impact ionization cross-sections and the kinetics of ion–molecule reactions of *2*-C_4F_8. Possible dissociative ionization channels will be discussed on thermochemical grounds. Status of theory is that binary encounter Bethe [14] (BEB) predicts total cross-sections but not the individual dissociative ionization channels. The present results therefore form a validating data set for new theoretical developments.

2. Experimental

All of the experiments were performed using a modified Extrel FTMS equipped with a cubic ion cyclotron resonance trapping cell (5 cm on a side) and a 2-T superconducting magnet [15]. The theory and methodology of FTMS have been well documented in the literature [16–18]. For the ionization cross-section measurements, *2*-C_4F_8 (>99%, Matheson) and Ar (99.999%, Matheson) are mixed in a manifold, at a ratio of about 1:1, with the pressure ratio determined by capacitance manometry. Ar is used as a calibration standard for assigning absolute values to the measured ionization

* Corresponding author. Tel.: +1 937 2552246; fax: +1 937 6564657.
E-mail address: alan.garscadden@wpafb.af.mil (A. Garscadden).

1387-3806/$ – see front matter. Published by Elsevier B.V.
doi:10.1016/j.ijms.2008.04.007

cross-sections, as will be discussed later. The mixture is then admitted through a precision leak valve (Varian-controlled leak valve) into the FTMS system. Ions are formed by electron impact in the trapping cell at pressures in the 10^{-7} torr range. An electron gun (Kimball Physics ELG2, Wilton, NH) irradiates the cell with a few hundred picocoulombs of low-energy electrons (detailed description of the electron beam is given below). The motion of the ions is constrained radially by the superconducting magnetic field and axially by an electrostatic potential (trapping potential) applied to the trap faces that are perpendicular to the magnetic field. The trapping potential is usually set to 10 V (see below for more details about the potential profile in the trapping cell). Ions of all mass-to-charge ratios are simultaneously and coherently excited into cyclotron orbits using stored waveform inverse Fourier transform (SWIFT) [19–21] applied to two opposing trap faces which are parallel to the magnetic field. Following cyclotron excitation, the image currents induced on the two remaining faces of the trap are amplified, digitized and Fourier analyzed to yield a mass spectrum. The intensity ratios of the ions from *2*-C_4F_8 to Ar^+ give cross-sections relative to those for electron impact ionization of Ar [22] since the pressure ratio of *2*-C_4F_8 to Ar is known—the pressure ratio of *2*-C_4F_8 to Ar in the trapping cell region is equal to the pressure ratio in the manifold, as discussed in our previous paper [23].

To study the reactions of ions, generated from electron impact ionization, with the parent molecule, a mixture of *2*-C_4F_8 and Ar with a ratio of ~1:20 was used. The ion to be studied is selected by using SWIFT to eject other ions out of the trapping cell, followed by a cooling period in which the ion undergoes multiple collisions with Ar at a total pressure of $\sim 1 \times 10^{-5}$ torr for various times, typically 500 ms. SWIFT is used again to select the ion to be studied from others that are formed during the cooling period, followed by a programmed reaction time varying from 0 to 1000 ms. The cooling period serves two purposes: (1) excited ions are thermalized by collisions with Ar atoms, and/or (2) excited ions with reaction rates greater than the ground state ions are exhausted. The pressure of Ar and the length of the cooling period are adjusted so that at the end of the cooling period there are still sufficient reactant ions to study and their reaction shows a single exponential decay to the end of the reaction time, at which time only a few percent of the reactant ions remain. With the large Ar partial pressure, Ar^+ is overpopulated during the electron impact ionization, resulting in a significant space charge effect. To eliminate this effect, a single frequency rf waveform is applied during the electron beam event to continuously eject Ar^+ out of the trapping cell.

The trapping cell of the Extrel FTMS has been modified by adding a screen electrode in front of each trapping plate, for the purpose of improving the trapping potential profile in the cell. Wang and Marshall have given a detailed description of the design of the screen electrodes [24]. With the screen electrodes, which are held at ground potential, a particle-in-a-box potential profile (rather than a harmonic oscillator potential profile) in the trapping cell can be achieved [25]. When the trapping potential is set to 10 V as mentioned above, the potential drop within the screen electrode region is estimated to be 0.3 V. In comparison, without the screen electrodes, even at trapping potential of 2 V, the potential drop across the two trapping plates will be ~0.5 V. The potential drop in the trapping cell changes the electron energy depending on where the electron ionizes the gas molecule and thus affects the uncertainty of the ionizing electron energies; the greater the potential drop, the larger the energy spread in the electron beam. In summary, the benefit of using the screen electrodes is that it allows us to apply high trapping potentials (up to 10 V) to trap more kinetically energetic ions (in theory, ions with kinetic energy up to 9.7 eV can be trapped), while in most of the cell volume the potential drop is small enough to avoid broadening of the electron energy distribution in the beam.

The Kimball Physics ELG-2 electron gun is rated for energies of 10–1000 eV with beam currents of 1 nA to 3 μA. The energy spread of the beam is about 0.25 eV plus the space charge well of the beam [26]. Combining the electron energy spread in the electron source and the potential drop in the trapping cell mentioned above, we estimate the uncertainty of the ionizing electron energies in the FTMS trapping cell to be ±0.6 eV.

3. Results and discussion

Electron impact ionization of *2*-C_4F_8 produces 15 ions including CF_{1-3}^+, $C_2F_{1-4}^+$, $C_3F_{1-6}^+$ and $C_4F_{7,8}^+$. The ionization cross-sections for these ions, as functions of the electron energy in a range of 10–200 eV, are shown in Fig. 1. A variety of energy dependences for partial cross-sections can be seen, e.g., cross-sections peak at different electron energies. While cross-sections for lighter fragment ions reach their maxima at ~100 eV or higher and display a broad-peak profile, cross-sections for heavier fragment ions as well as the parent ion peak at 40 eV or lower energies. For the parent ion $C_4F_8^+$, the cross-section increases sharply above the threshold, reaching a maximum at ~25 eV, and then decreasing rapidly at higher energies. For reference, the total cross-section reaches a maximum at 90 eV with a value of 1.2×10^{-15} cm^2. We interpret the behavior of the heavy fragment ions and the parent ion, i.e., their cross-sections starting to decline before the maximum total cross-section, as the result of their further fragmentation at higher electron energies. The formation of the parent ion $C_4F_8^+$ is the major ionization channel from threshold to 18 eV. This result of the electron impact ionization is in agreement with the photoionization results in Jarvis et al.'s study on threshold photoelectron–photoion coincidence spectroscopy of *2*-C_4F_8, in which they found that the ground state of *2*-$C_4F_8^+$ is bound in the Frank–Condon region [27]. Above 18 eV and below 70 eV, $C_3F_5^+$ becomes the most abundant ion. Other important ions at low energies include CF_3^+, $C_4F_7^+$, $C_3F_6^+$, $C_2F_4^+$ and $C_3F_3^+$. At higher energies, small ions such as CF^+ and CF_2^+ also become significant. Above 70 eV, CF_3^+ dominates the product ion population. Cross-section data for the above nine most abundant ions are shown in Table 1. The maximum in the total ionization cross-section of *2*-C_4F_8 is smaller than that of *c*-C_4F_8 which we previously measured as 1.6×10^{-15} cm^2, although the two measurements are within the combined absolute uncertainties [13]. Furthermore, in *c*-C_4F_8 both $C_2F_4^+$ and $C_3F_5^+$ are equally abundant ions over the energy range of 10–200 eV [13], while in *2*-C_4F_8, $C_2F_4^+$ is far less significant than $C_3F_5^+$.

The uncertainty in the FTMS experimental data is estimated to be ±14%, which includes those contributions from the pressure measurements (mainly due to the deviation of the pressure ratio of *2*-C_4F_8 to Ar in the trapping cell from that in the manifold, see Ref. [23]) and the ion intensity measurements (mainly due to the mass discrimination resulting from space charge effects and errors in excitation and detection of ions). When combined with the uncertainty of ±3.5% in the Ar cross-section for calibration [22], the overall uncertainty in the cross-section data reported in this paper is ±18%. Table 2 lists detailed estimated uncertainties for each possible source of error mentioned above. For minor ions with rather small cross-sections the uncertainties are higher due to their lower signal-to-noise ratios in the mass spectra. Uncertainty due to the loss of ions from the trapping cell is negligible compared to the other source of errors, since the FTMS trapping cell has been modified for improved trapping efficiency (see Section 2) and that the kinetic energy of ions formed in our experiments is most likely less than a few eV [28].

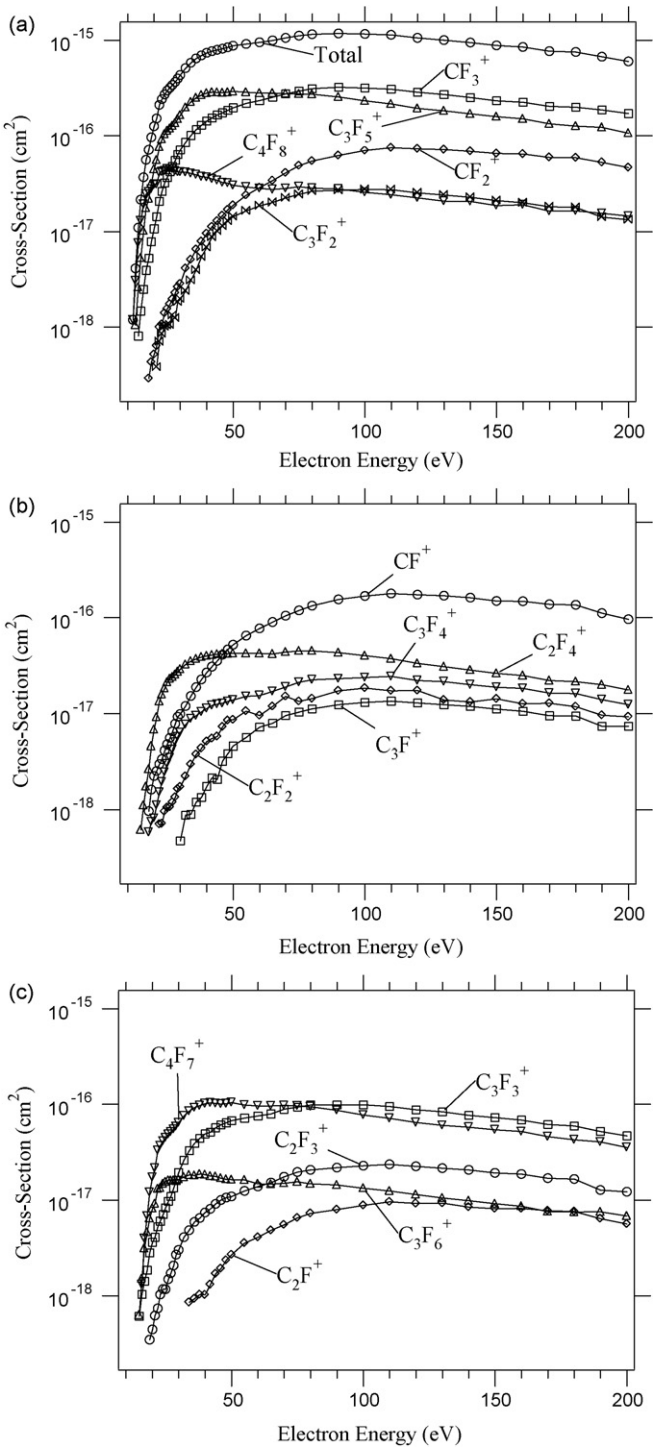

Fig. 1. Cross-sections of electron impact ionization of *2*-C_4F_8. For visual clarity data are presented in plots (a)–(c), in which scales are set to the same for easy comparison of amplitudes of different ionization channels. Combined with the uncertainty in the reference cross-section of Ar for calibration, the estimated uncertainty is ±18%. The scatter in the data in some cross-section curves may be due to the statistical fluctuations rather than fine structure in the cross-section profiles.

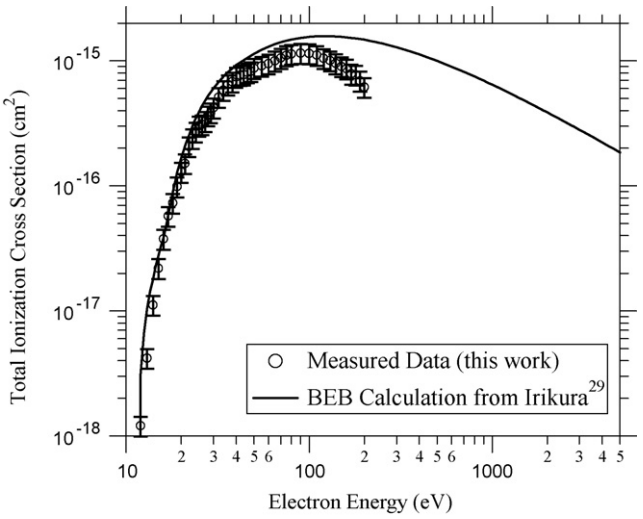

Fig. 2. Comparison between the measured total ionization cross-section in this work and the theoretical ionization cross-section calculated by Irikura [29] using binary encounter Bethe (BEB) model [30]. Error bars indicate ±18% uncertainties in our measurement.

In Fig. 2 the total ionization cross-section determined by our FTMS experiments is compared to the theoretical ionization cross-section calculated by Irikura [29] using BEB model [30]. There is excellent agreement between the data up to approximately 50 eV but there is an obvious deviation between the experimental data and the theoretical data in the high energy range, which is beyond the estimated uncertainty of the FTMS data. The discrepancy at high energy might be explained by the formation of energetic fragment ions from doubly charged ions which dissociate to two monocations. These energetic ions could conceivably escape the trapping potential of the FTMS and failed to be accounted for. To check this hypothesis, Irikura [29] recalculated the BEB cross-section ignoring the possibility of double ionization. While this indeed brought the calculated cross-section closer to the measured data, the maximum change was only 10% at 200 eV, which was not enough to bring the two data sets in line. Therefore, at this point we cannot explain the discrepancy between the measured and BEB cross-section at higher energies.

In Table 3, we look more closely at the dissociative ionization channels of *2*-C_4F_8 for the nine most abundant fragment ions. Table 3 presents most of the reasonable fragmentation pathways for the formation of each fragment ion, and the calculated reaction enthalpies using thermochemical data from the literature [27,31–36] as complied in Table 4. The reaction enthalpies are then compared to the observed appearance energies (AE) to assess their probability on thermochemical grounds. Fragment ions in Table 3 are listed in the order of decreasing mass, and for any given ion the formation channels, numbered (1)–(32), include the direct fragmentation of the parent ion as well as subsequent fragmentation of the larger daughter ions by spontaneous unimolecular dissociation. For example, $C_2F_4^+$ can be formed from direct dissociation of $C_4F_8^+$ (11), or from further dissociation of $C_4F_7^+$. In this case reaction (2) leads to $C_4F_7^+ + F + 2e^-$, followed by unimolecular dissociation of $C_4F_7^+ \rightarrow C_2F_4^+ + C_2F_3$. These two steps taken together are shown as reaction (12) in Table 3. In a similar manner, reaction (3) leads to $C_3F_6^+ + CF_2 + 2e^-$, followed by spontaneous dissociation of $C_3F_6^+$ yielding $C_2F_4^+ + CF_2$, the two steps shown as (13). Finally, $C_2F_4^+$ can also be formed from the formation of $C_3F_5^+$ (6) and its subsequent fragmentation giving the net reaction (14). From Table 3 one can see that $C_3F_6^+$ and $C_3F_5^+$ should not be in cyclic forms, as their reaction enthalpies are greater than the appearance energies of these ions. The knowledge of $C_3F_6^+$ and $C_3F_5^+$ being linear structures will be useful later for calculations of the thermochemical data of various ion–molecule reactions. Based on the comparison of the reaction enthalpies and the ion appearance energies, within the uncertainties of the calculated enthalpies, we conclude that $C_3F_6^+$, $C_3F_5^+$, $C_2F_4^+$ and CF_3^+ are formed by primary fragmentation

Table 1
Partial cross-sections (10^{-16} cm^2) of electron impact ionization of *2*-C_4F_8 for the production of the nine most abundant ions

Energy (eV)	$C_4F_8^+$	$C_4F_7^+$	$C_3F_6^+$	$C_3F_5^+$	$C_3F_3^+$	$C_2F_4^+$	CF_3^+	CF_2^+	CF^+	Total
10										
11										
12	0.01									0.01
13	0.03			0.01						0.04
14	0.08			0.03			0.01			0.12
15	0.13		0.01	0.05	0.01	0.01	0.01			0.22
16	0.19	0.01	0.02	0.10	0.01	0.01	0.02			0.37
17	0.25	0.04	0.03	0.18	0.01	0.02	0.04			0.56
18	0.26	0.07	0.05	0.22	0.02	0.03	0.05	0.003	0.01	0.71
19	0.28	0.12	0.06	0.32	0.03	0.05	0.08	0.004	0.02	0.96
20	0.30	0.17	0.08	0.45	0.04	0.07	0.11	0.005	0.02	1.26
21	0.31	0.21	0.09	0.56	0.04	0.09	0.14	0.006	0.03	1.51
22	0.41	0.33	0.13	0.76	0.05	0.13	0.21	0.01	0.03	2.10
23	0.42	0.37	0.13	0.92	0.06	0.16	0.26	0.01	0.03	2.41
24	0.43	0.41	0.15	1.04	0.07	0.18	0.32	0.01	0.04	2.72
25	0.45	0.45	0.16	1.13	0.08	0.21	0.37	0.02	0.05	2.97
26	0.45	0.49	0.16	1.19	0.10	0.23	0.42	0.02	0.06	3.18
27	0.45	0.52	0.16	1.27	0.11	0.24	0.48	0.02	0.06	3.39
28	0.43	0.55	0.16	1.37	0.13	0.26	0.55	0.02	0.08	3.65
29	0.42	0.59	0.16	1.49	0.16	0.27	0.64	0.03	0.09	3.97
30	0.42	0.64	0.16	1.64	0.19	0.29	0.71	0.03	0.10	4.33
32	0.41	0.76	0.17	1.98	0.26	0.33	0.85	0.04	0.12	5.09
34	0.40	0.85	0.18	2.26	0.33	0.35	1.01	0.05	0.15	5.81
36	0.39	0.93	0.18	2.51	0.39	0.37	1.16	0.06	0.19	6.44
38	0.37	0.97	0.19	2.68	0.44	0.39	1.29	0.08	0.23	6.93
40	0.37	1.02	0.18	2.80	0.49	0.40	1.43	0.10	0.27	7.39
42	0.35	1.03	0.18	2.86	0.51	0.41	1.54	0.11	0.31	7.68
44	0.34	1.03	0.18	2.84	0.57	0.42	1.65	0.13	0.35	7.92
46	0.32	1.01	0.17	2.82	0.61	0.42	1.75	0.15	0.41	8.13
48	0.32	1.02	0.16	2.86	0.64	0.42	1.85	0.17	0.47	8.43
50	0.30	1.04	0.16	2.91	0.68	0.42	1.97	0.19	0.52	8.75
55	0.29	0.98	0.16	2.86	0.72	0.42	2.18	0.24	0.65	9.15
60	0.28	0.96	0.15	2.81	0.76	0.42	2.34	0.29	0.77	9.47
65	0.27	0.96	0.15	2.80	0.79	0.42	2.53	0.34	0.90	9.94
70	0.28	0.97	0.15	2.77	0.89	0.44	2.74	0.41	1.05	10.59
75	0.29	0.96	0.15	2.76	0.94	0.45	2.94	0.49	1.19	11.12
80	0.28	0.94	0.15	2.72	0.98	0.45	3.11	0.55	1.34	11.55
90	0.28	0.87	0.14	2.55	0.99	0.43	3.22	0.63	1.56	11.76
100	0.26	0.77	0.13	2.33	0.99	0.40	3.17	0.71	1.69	11.59
110	0.24	0.71	0.12	2.17	0.95	0.37	3.08	0.75	1.79	11.35
120	0.23	0.64	0.11	1.94	0.87	0.33	2.85	0.73	1.74	10.56
130	0.21	0.61	0.10	1.82	0.84	0.31	2.71	0.72	1.70	10.04
140	0.21	0.58	0.10	1.70	0.77	0.28	2.51	0.69	1.62	9.43
150	0.19	0.54	0.09	1.59	0.73	0.26	2.32	0.65	1.50	8.81
160	0.19	0.52	0.09	1.51	0.68	0.25	2.25	0.65	1.48	8.51
170	0.16	0.46	0.08	1.33	0.62	0.22	2.04	0.60	1.38	7.70
180	0.16	0.43	0.07	1.27	0.60	0.21	2.00	0.59	1.37	7.50
190	0.15	0.41	0.08	1.22	0.52	0.20	1.86	0.53	1.11	6.72
200	0.15	0.35	0.07	1.06	0.47	0.18	1.71	0.47	0.96	6.02

The total ionization cross-section is also included.

(i.e., fragmentation directly from the parent ion $C_4F_8^+$), with neutral partners of CF_2 (3), CF_3 (6), C_2F_4 (11) and C_3F_5 (15), respectively. Our conclusion of $C_3F_5^+$ and CF_3^+ being formed by primary fragmentation of $C_4F_8^+$ is in agreement with results from the study by Jarvis et al. in which they found that the removal of an electron from a C–C σ-bonding orbital of *2*-C_4F_8 upon photoionization weakens the C–C bond and results in fragment ions of $C_3F_5^+$ and CF_3^+ [27]. Given this scenario, the formation of $C_3F_5^+$ and CF_3^+ are likely to be competing channels, and since both ions are observed at low electron energies (actually $C_3F_5^+$ has greater intensity than CF_3^+), $C_3F_5^+$ should have an ionization energy (IE) close to that of CF_3^+, if not lower, as implied by Stevenson's rule which states that the positive charge will remain on the fragment of lower ionization potential [37]. Using heat of formation (ΔH_f) data in Table 4, IE(CF_3^+) is calculated to be 8.9 eV, and IE($C_3F_5^+$), to be 9.3 ± 0.4 eV, the uncertainty derived from that of $\Delta H_f(C_3F_5^+) = 134 \pm 42$ kJ/mol in Table 4. We therefore believe that the lower limit of 134 ± 42 kJ/mol is more appropriate for $\Delta H_f(C_3F_5^+)$—so that IE($C_3F_5^+$) ≅ IE(CF_3^+). We will refer to this result later when enthalpies of ion–molecule reactions are discussed. For $C_3F_3^+$, the reaction enthalpy cannot be calculated because of the lack of relevant thermochemical data and therefore no definitive formation channel can be suggested. It is unlikely, however, that the ion is formed by primary fragmentation (not listed in Table 3) because that would result in a neutral partner of CF_5. Reasonable channels include secondary fragmentation of $C_4F_7^+$ (9) or $C_3F_5^+$ (10). The determination of the fragmentation channels for CF_2^+ and CF^+ is even less certain. For CF_2^+, possible formation channels on thermochemical grounds include a primary fragmentation (20) and a secondary fragmentation (22). If (20), the difference between the observed appearance energy and the calculated reaction enthalpy will be 3.8 eV—which for a primary fragmentation process it is too large to be explained by an intrinsic kinetic shift [38]. Reactions (20) and (3) forming CF_2^+ and $C_3F_6^+$, respectively, both as primary fragmentations, are likely to be via the same fragmentation processes, with the positive charge staying with different moieties, respectively, and therefore (20) is

not expected to occur, according to Stevenson's rule [37], because IE(CF_2^+) = 11.4 ± 0.1 eV is greater than IE($C_3F_6^+$) = 10.6 eV, calculated using thermochemical data in Table 4. Basing on the above discussion we propose that the most likely channel forming CF_2^+ is reaction (22), a secondary fragmentation. For CF^+, several primary and secondary fragmentation processes are possible on thermochemical grounds, but the three secondary fragmentations, (26), (28), and (29) are more likely because the reaction enthalpies are in better agreement with the appearance energy. A mass spectrometer study on collision-induced dissociation (CID) of ions from *2*-C_4F_8 has found that CF_2^+ is produced by CID of $C_2F_4^+$, and that CF^+ is produced by CID of $C_3F_5^+$ or $C_2F_4^+$ [39], providing support to the above proposed channels for the formation of CF_2^+ and CF^+, i.e., via the secondary fragmentation pathways (22) and (29), respectively.

Ion–molecule reactions were studied for all of the ions listed in Table 3. Among these ions only the lightest ions, CF_{1-3}^+, are found to react with their parent molecule *2*-C_4F_8 forming $C_4F_8^+$ by charge transfer or $C_4F_7^+$ by F^- transfer, as shown in Table 5 and indicated by non-zero rate coefficients. We observed no reaction between $C_4F_8^+$ and C_4F_8 but our observation cannot rule out the possibility of symmetric charge transfer between $C_4F_8^+$ and C_4F_8. The rate coefficients are derived from our measured relative rate coefficients which are calibrated against Morris et al.'s reaction rate coefficients for CF_3^+ + *2*-C_4F_8 [40]. Reaction of CF^+, CF_2^+ or CF_3^+ with *2*-C_4F_8 forming $C_4F_7^+$ is said to be via F^- transfer because the alternative mechanism, dissociative charge transfer, would be endothermic for these ions, by 491 ± 47, 268 ± 51 and 511 ± 39 kJ/mol, respectively, using thermochemical data in Table 4. To understand what governs the observed reactivities of these ions, we have calculated the reaction enthalpies for all possible charge transfer and F^- transfer reactions using the data in Table 4, including non-reactive ions. The heat of formation of $C_3F_3^+$ is not known from the literature, but if our observed AE($C_3F_3^+$/*2*-C_4F_8) = 15 eV (Table 3) is used, $\Delta H_f(C_3F_3^+)$ can be estimated to be 310 kJ/mol, and therefore the reaction enthalpy for F^- transfer from $C_3F_3^+$, is 387 ± 39 kJ/mol. Although some of the calculated reaction enthalpies have rather

Table 2
Estimated uncertainties in ionization cross-section data contributed from possible sources of errors in FTMS experiments

Pressure ratio[a]	±5%
Electronics[b]	±6%
Space charge[c]	±3%
Ar^+ cross-section[d]	±3.5%
Total	±18%

[a] Mainly due to the deviation of the pressure ratio of *2*-C_4F_8 to Ar in the trapping cell to that in the manifold, see Ref. [23].
[b] Includes errors from r.f. function generator for excitation, amplifier for excitation and preamplifier for detection.
[c] Space charge effect is estimated by the linearity of measured ion intensity vs. expected ion population.
[d] Uncertainty in ionization cross-section of Ar [22] which is used as a calibration standard for the cross-sections measured in this experiment.

Table 3
Ionization channels and their reaction enthalpies (ΔH_{rxn}), calculated using the thermochemical data in Table 4, unless otherwise indicated

Ion/AE	Possible channel		Most likely channel	ΔH_{rxn} (eV)
$C_4F_8^+$/12 eV	2-C_4F_8 + e^- → $C_4F_8^+$ + 2e^-	(1)		11.1
$C_4F_7^+$/16 eV	2-C_4F_8 + e^- → $C_4F_7^+$ + F + 2e^-	(2)	*Primary	14.2 ± 0.4[a]
$C_3F_6^+$/15 eV	2-C_4F_8 + e^- → $C_3F_6^+$ + CF_2 + 2e^-	(3)	*Primary	13.4 ± 0.1
	2-C_4F_8 + e^- → *c*-$C_3F_6^+$ + CF_2 + 2e^-	(4)		15.5 ± 0.1
	2-C_4F_8 + e^- → $C_3F_6^+$ + CF + F + 2e^-	(5)		19.0 ± 0.1
$C_3F_5^+$/13 eV	2-C_4F_8 + e^- → $C_3F_5^+$ + CF_3 + 2e^-	(6)	*Primary	13.2 ± 0.4
	2-C_4F_8 + e^- → *c*-$C_3F_5^+$ + CF_3 + 2e^-	(7)		15.0
	2-C_4F_8 + e^- → $C_3F_5^+$ + CF_2 + F + 2e^-	(8)		20.9 ± 0.6
$C_3F_3^+$/15 eV	2-C_4F_8 + e^- → $C_3F_3^+$ + CF_4 + F + 2e^-	(9)	*Secondary	–[b]
	2-C_4F_8 + e^- → $C_3F_3^+$ + F_2 + CF_3 + 2e^-	(10)	*Secondary	–[b]
$C_2F_4^+$/15 eV	2-C_4F_8 + e^- → $C_2F_4^+$ + C_2F_4 + 2e^-	(11)	*Primary	13.0 ± 0.03
	2-C_4F_8 + e^- → $C_2F_4^+$ + C_2F_3 + F + 2e^-	(12)		18.7 ± 0.1
	2-C_4F_8 + e^- → $C_2F_4^+$ + 2CF_2 + 2e^-	(13)		15.6 ± 0.2
	2-C_4F_8 + e^- → $C_2F_4^+$ + CF + CF_3 + 2e^-	(14)		17.7 ± 0.1
CF_3^+/14 eV	2-C_4F_8 + e^- → CF_3^+ + C_3F_5 + 2e^-	(15)	*Primary	12.8
	2-C_4F_8 + e^- → CF_3^+ + C_3F_4 + F + 2e^-	(16)		15.4
	2-C_4F_8 + e^- → CF_3^+ + C_2F_3 + CF_2 + 2e^-	(17)		16.5 ± 0.2
	2-C_4F_8 + e^- → CF_3^+ + C_2F_2 + CF_3 + 2e^-	(18)		16.1 ± 0.2
	2-C_4F_8 + e^- → CF_3^+ + CF + C_2F_4 + 2e^-	(19)		16.5 ± 0.1
CF_2^+/18 eV	2-C_4F_8 + e^- → CF_2^+ + C_3F_6 + 2e^-	(20)		14.2
	2-C_4F_8 + e^- → CF_2^+ + C_3F_5 + F + 2e^-	(21)		19.7
	2-C_4F_8 + e^- → CF_2^+ + C_2F_4 + CF_2 + 2e^-	(22)	*Secondary	16.9 ± 0.2
	2-C_4F_8 + e^- → CF_2^+ + C_2F_3 + CF_3 + 2e^-	(23)		19.1 ± 0.1
CF^+/18 eV	2-C_4F_8 + e^- → CF^+ + *n*-C_3F_7 + 2e^-	(24)		15.2
	2-C_4F_8 + e^- → CF^+ + *i*-C_3F_7 + 2e^-	(25)		14.6
	2-C_4F_8 + e^- → CF^+ + C_3F_6 + F + 2e^-	(26)	*Secondary	17.5
	2-C_4F_8 + e^- → CF^+ + C_3F_5 + F_2 + 2e^-	(27)		20.4
	2-C_4F_8 + e^- → CF^+ + C_2F_5 + CF_2 + 2e^-	(28)	*Secondary	16.9 ± 0.2
	2-C_4F_8 + e^- → CF^+ + C_2F_4 + CF_3 + 2e^-	(29)	*Secondary	16.7
	2-C_4F_8 + e^- → CF^+ + C_2F_2 + CF_4 + F + 2e^-	(30)		19.7 ± 0.2
	2-C_4F_8 + e^- → CF^+ + C_2F_2 + F_2 + CF_3 + 2e^-	(31)		23.8 ± 0.2
	2-C_4F_8 + e^- → CF^+ + F + C_2F_4 + CF_2 + 2e^-	(32)		20.2 ± 0.2

Ions are listed in the order of decreasing mass, along with the observed appearance energy (AE). The most likely formation channel(s) for each fragment ion is marked by an asterisk (*) with the type of the fragmentation, primary or secondary (see the text), indicated.
[a] Cited from the appearance energy measurement by Ref. [27].
[b] Heat of formation of $C_3F_3^+$ is not known from the literature.

Table 4
Thermochemical data for fluorocarbon species, cited from the compilation of Lias et al. [29]

Neutrals	ΔH_f (kJ/mol)	Ions	ΔH_f (kJ/mol)
2-C_4F_8	−1597	$C_4F_8^+$	−526
c-C_4F_8	−1542.6[a]	$C_4F_7^+$	−306 ± 39[b]
n-C_3F_7	−1269[c]	$C_3F_6^+$	−102
i-C_3F_7	−1325[c]	c-$C_3F_6^+$	101
C_3F_6	−1125	$C_3F_5^+$	134 ± 42[d]
c-C_3F_6	−978	c-$C_3F_5^+$	307[e]
C_3F_5	−762[f]	$C_2F_4^+$	316
C_3F_4	−594	$C_2F_3^+$	791
C_2F_6	−1343	CF_3^+	399.0
C_2F_5	−893 ± 4	CF_2^+	897
C_2F_4	−659 ± 3	CF^+	1134.2
C_2F_3	−192.0 ± 8.4		
C_2F_2	−21 ± 21		
CF_4	−934.5 ± 0.4		
CF_3	−460		
CF_2	−205 ± 12		
CF	255.2 ± 8		
F	79.4 ± 0.3		

Except for those otherwise indicated.
[a] From Ref. [32].
[b] Calculated using AE($C_4F_7^+$/2-C_4F_8) = 14.2 ± 0.4 eV from Ref. [27] and ΔH_f for 2-C_4F_8 and F in this table.
[c] From Ref. [33].
[d] From Ref. [34].
[e] Calculated using AE(c-$C_3F_5^+$/c-C_3F_6) = 14.14 eV from Ref. [35], and ΔH_f for C_3F_6, c-C_3F_6 and F in this table.
[f] From Ref. [36].

large combined uncertainties, such as 32 ± 81 kJ/mol for F^- transfer from $C_3F_5^+$, the overall data indicate that all channels that are exothermic are all observed to occur; channels that are not observed to occur are all endothermic—it suggests that these two types of reactions, charge transfer and F^- transfer, are basically thermochemically controlled, in contrast to a hypothetical CF_3^- transfer reaction as mentioned below. We note that if the lower limit of $\Delta H_f(C_3F_5^+)$ in Table 4, as mentioned earlier, is used, the $C_3F_5^+$ reaction enthalpy will be even more endothermic.

Table 5
Possible charge transfer (CT) and fluoride transfer (FT) reactions of selected fluorocarbon ions with 2-C_4F_8

Reactants	Products	Rate coefficient (10^{10} cm^3/s)	ΔH_{rxn} (kJ/mol)
$C_4F_7^+$ + 2-C_4F_8	→ $C_4F_8^+$ + C_4F_7 (CT)	0	–[a]
$C_3F_6^+$ + 2-C_4F_8	→ $C_4F_7^+$ + C_3F_7 (FT)	0	124 ± 81[b], 68 ± 81[c]
	→ $C_4F_8^+$ + C_3F_6 (CT)	0	48
$C_3F_5^+$ + 2-C_4F_8	→ $C_4F_7^+$ + C_3F_6 (FT)	0	32 ± 81
	→ $C_4F_8^+$ + C_3F_5 (CT)	0	175 ± 42
$C_3F_3^+$ + 2-C_4F_8	→ $C_4F_7^+$ + C_3F_4 (FT)	0	387 ± 39[d]
	→ $C_4F_8^+$ + C_3F_3 (CT)	0	–[e]
$C_2F_4^+$ + 2-C_4F_8	→ $C_4F_7^+$ + C_2F_5 (FT)	0	82 ± 46
	→ $C_4F_8^+$ + C_2F_4 (CT)	0	96 ± 3
CF_3^+ + 2-C_4F_8	→ $C_4F_7^+$ + CF_4 (FT)	6.8[f]	−43 ± 39
	→ $C_4F_8^+$ + CF_3 (CT)	0	212
CF_2^+ + 2-C_4F_8	→ $C_4F_7^+$ + CF_3 (FT)	9.9	−66 ± 39
	→ $C_4F_8^+$ + CF_2 (CT)	4.2	−31 ± 12
CF^+ + 2-C_4F_8	→ $C_4F_7^+$ + CF_2 (FT)	13.3	−48 ± 51
	→ $C_4F_8^+$ + CF (CT)	0	192 ± 8

Actually observed reactions are indicated by the non-zero reaction rate coefficients. Also included are the reaction enthalpies (ΔH_{rxn}) calculated using the thermochemical data in Table 4 unless otherwise indicated.
[a] Heat of formation of C_4F_7 is not known.
[b] For n-C_3F_7 to be the neutral product.
[c] For i-C_3F_7 to be the neutral product.
[d] Heat of formation of $C_3F_3^+$ is not know from the literature, but we estimated it to be 310 kJ/mol (see the text).
[e] Heat of formation of C_3F_3 is not known from the literature.
[f] Calibration point (see text).

It is interesting to compare the ion–molecule reactions in 2-C_4F_8 and in c-C_4F_8. While in 2-C_4F_8 only F^- and charge transfers are involved, in c-C_4F_8 a variety of reaction types is involved, with major channels producing $C_3F_5^+$.[13] The reactions between c-C_4F_8 and CF_2^+ or $C_2F_3^+$, the only two ions that react,[13] may proceed through the following possible channels to produce $C_3F_5^+$.

$$CF_2^+ + c\text{-}C_4F_8 \rightarrow C_3F_5^+ + CF_3 + CF_2 \quad (33)$$

or

$$CF_2^+ + c\text{-}C_4F_8 \rightarrow C_3F_5^+ + C_2F_5 \quad (34)$$

$$C_2F_3^+ + c\text{-}C_4F_8 \rightarrow C_3F_5^+ + CF_3 + C_2F_3 \quad (35)$$

or

$$C_2F_3^+ + c\text{-}C_4F_8 \rightarrow C_3F_5^+ + C_3F_6 \quad (36)$$

The dissociative charge transfer reactions (33) and (35) can be ruled out because they are endothermic by 114.6 + 54 and 233.6 + 50.4 kJ/mol, respectively, calculated using thermochemical data in Table 4. On the other hand, reactions (34) and (36) are exothermic by 113.4 + 46 and 239.4 + 42 kJ/mol, respectively. These two reactions can be viewed as a C_2F_3 transfer reaction (34), a CF_2 transfer reaction (36), or a CF_3^- transfer reaction (both). The fact that $C_3F_5^+$ is the common product ion for both reactions of CF_2^+ and $C_2F_3^+$ suggests the CF_3^- transfer as the more likely mechanism. Why different dominant reaction mechanisms are involved in 2-C_4F_8 and in c-C_4F_8 is a topic worthy of further investigation. The lack of CF_3^- transfer in 2-C_4F_8 reactions cannot be explained on thermochemical grounds, because the reaction enthalpies for CF^+, CF_2^+ and CF_3^+ undergoing CF_3^- transfer with 2-C_4F_8 are −62 ± 42, −59 ± 46 and −11 ± 42 kJ/mol as calculated using data in Table 4. We note that the uncertainties in these values primarily originate from that of $\Delta H_f(C_3F_5^+)$, and if the lower limit of $\Delta H_f(C_3F_5^+)$ is used, these reaction enthalpies will be more exothermic.

Ar^+ reaction with 2-C_4F_8 were also studied, as Ar is frequently used as a diluent in etching reactors. This reaction yields the following product ions:

$$Ar^+ + 2\text{-}C_4F_8 \rightarrow C_4F_7^+ + F + Ar \quad (82\%) \quad (37)$$

$$Ar^+ + 2\text{-}C_4F_8 \rightarrow C_3F_5^+ + CF_3 + Ar \quad (9\%) \quad (38)$$

$$Ar^+ + 2\text{-}C_4F_8 \rightarrow C_3F_6^+ + CF_2 + Ar \quad (7\%) \quad (39)$$

$$Ar^+ + 2\text{-}C_4F_8 \rightarrow C_4F_8^+ + Ar \quad (2\%) \quad (40)$$

with branching ratios shown in parentheses. The reaction rate coefficient is 2.3×10^{-9} cm^3/s and as can be seen from the table, produces predominantly $C_4F_7^+$ with F radical as the neutral partner. At higher power densities in an etching plasma Ar will be significantly ionized and become an important source term for $C_4F_7^+$ and atomic F (reaction (37)). For the Ar^+ reaction with c-C_4F_8, the rate coefficient is 1.4×10^{-9} cm^3/s with $C_2F_4^+$ and $C_3F_5^+$ the two equally major product ions [13].

4. Summary

2-C_4F_8 is one of the promising candidates to replace c-C_4F_8 as an etching gas, widely used in the semiconductor industry for dielectric etch, but not environmentally friendly. In this study, the dominant ions produced by electron impact ionization of 2-C_4F_8 are the parent ion, $C_4F_8^+$, from threshold to 18 eV, and $C_3F_5^+$ from 18 to 70 eV. The total ionization cross-section for 2-C_4F_8 reaches a

maximum of 1.2×10^{-15} cm^2 at 90 eV. For comparison, the ionization of *c*-C_4F_8, which we have studied previously, yields no parent ion but two equally dominant ions $C_2F_4^+$ and $C_3F_5^+$ throughout the energy range from 10 to 200 eV and a total ionization cross-section of 1.6×10^{-15} cm^2 at approximately the same energy.[13] $C_3F_5^+$ is believed to be formed from *2*-C_4F_8 with production of the neutral partner CF_3. Other significant ions from electron impact ionization of *2*-C_4F_8 at low energies include CF_3^+, $C_4F_7^+$, $C_3F_6^+$, $C_2F_4^+$ and $C_3F_3^+$, of which the neutral partner of the first four are C_3F_5, F, CF_2 and C_2F_4, respectively. For $C_3F_3^+$, neutral partners may be (CF_4 + F) or (CF_3 + F_2), resulting from successive fragmentation rather than direct fragmentation from parent ion $C_4F_8^+$.

The charge transfer reaction of Ar^+ with *2*-C_4F_8 produces mainly $C_4F_7^+$, in comparison with Ar^+ + *c*-C_4F_8 which produces two equally major product ions $C_2F_4^+$ and $C_3F_5^+$ [13]. Other ion chemistries in *2*-C_4F_8 and *c*-C_4F_8 also differ: among the major ions from electron impact ionization of *2*-C_4F_8, only CF^+, CF_2^+ and CF_3^+ are found to react with *2*-C_4F_8, via F^- or charge transfer mechanisms, while among the ions from electron impact ionization of *c*-C_4F_8 only CF_2^+ or $C_2F_3^+$ react with *c*-C_4F_8, mainly via CF_3^- transfer mechanism [13]. CF^+ and CF_3^+ are believed to play an important roles in plasma etching with fluorocarbon gases [12]. We have shown that the production and loss of these ions are quite different in *2*-C_4F_8 and in *c*-C_4F_8.

Acknowledgements

The authors thank the Air Force Office of Scientific Research for support. We also thank Dr. Karl Irikura of NIST in Gaithersburg, MD, for providing the theoretical ionization cross-section data for *2*-C_4F_8 using the BEB model.

References

[1] C.H. Shin, C.J. Knag, A. Egami, M. Nakamura, 201st Meeting of the Electrochemical Society, Proceedings of the International Symposium on Plasma Processing XIV, Paper 426, Philadelphia, PA, May, 2002.
[2] L. Pruette, S. Karechi, R. Reif, T. Sparks, L. Beu, V. Vartanian, in: C.R. Simpson, L. Mendicino, K. Rajeshwar, J.M. Fenton (Eds.), Environmental Issues in the Electronics/Semiconductor Industries and Electronchemical/Photochemical Methods for Pollution Abatement, The Electronchemical Society Proceedings Series, Pennington, NJ, 1998.
[3] S. Karecki, L. Pruette, R. Reif, T. Sparks, L. Beu, V. Vartanian, J. Electrochem. Soc. 145 (1998) 4305.
[4] V. Mohindra, H.H. Sawin, M.T. Mocella, J.M. Cook, J. Flanner, O. Turnnel, in: G.S. Mathad, D.W. Hess, M. Engelhardt (Eds.), Plasma Processing, The Electronchemical Society Proceedings Series, Pennington, NJ, 1994.
[5] F. Illuzzi, R. d'Agostino, C. Cascarano, V. Colaprico, F. S Fracassi, Proceedings of the Sixth Annual International Semiconductor Environmental Safety and Health Conference, SIA, June, 1999.
[6] F. Fracassi, R. d'Agostino, J. Vac. Sci. Technol. B 16 (1998) 1867.
[7] S. Samukawa, K. Tsuda, Jpn. J. Appl. Phys. 2 37 (1998) L1095.
[8] S. Samukawa, T. Kukai, J. Vac. Sci. Technol. B 17 (1999) 2551.
[9] S. Samukawa, T. Kukai, J. Vac. Sci. Technol. B 17 (1999) 2463.
[10] R. Chatterjee, S. Karecki, L. Pruette, R. Reif, V. Vartianian, T. Sparks, in: G.S. Mathad (Ed.), Plasma Etching Processes for Sub-Quarter Micron Devices, The Electronchemical Society Proceedings Series, Pennington, NJ, 1999.
[11] Chatterjee, S. Karecki, R. Reif, V. Vartianian, T. Sparks, J. Electrochem. Soc. 149 (2002) G276.
[12] S. Nakamura, M. Itano, H. Aoyama, K. Shibahara, S. Yokoyama, M. Hirose, Jpn. J. Appl. Phys. 42 (2003) 5759.
[13] C.Q. Jiao, A. Garscadden, P.D. Haaland, Chem. Phys. Lett. 297 (1998) 121.
[14] W. Hwang, Y.-K. Kim, M.E. Rudd, J. Chem. Phys. 104 (1996) 2956.
[15] C.Q. Jiao, C.A. DeJoseph Jr., A. Garscadden, J. Vac. Sci. Technol. A 23 (2005) 1295.
[16] M.B. Comisarow, A.G. Marshall, Chem. Phys. Lett. 25 (1974) 282.
[17] A.G. Marshall, P.B. Grosshans, Anal. Chem. 63 (1991) 215A.
[18] Z. Liang, A.G. Marshall, Anal. Chem. 62 (1990) 70.
[19] A.G. Marshall, T.L. Wang, T.L. Ricca, J. Am. Chem. Soc. 107 (1985) 7983.
[20] S. Guan, Chem. Phys. 91 (1989) 775.
[21] L. Chen, A.G. Marshall, Int. J. Mass Spectrom. Ion Processes 79 (1987) 115.
[22] H.C. Straub, P. Renault, B.G. Lindsay, K.A. Smith, R.F. Stebbings, Phys. Rev. A 52 (1995) 1115.
[23] C.Q. Jiao, C.A. DeJoseph Jr., R. Lee, A. Garscadden, Int. J. Mass Spectrom. 257 (2006) 34.
[24] M. Wang, A.G. Marshall, Anal. Chem. 61 (1989) 1288.
[25] S. Guan, A.G. Marshall, Int. J. Mass Spectrom. Ion Processes 146–147 (1995) 261.
[26] ELG-2A Electron Gun Instruction Manual, Kimball Physics, Inc., Wilton, New Hampshire, 1986.
[27] G.K. Jarvis, K.J. Boyle, C.A. Mayhew, R.P. Tuckett, J. Phys. Chem. A 102 (1998) 3230.
[28] For more discussion about the kinetic energy of ions formed from electron impact ionization, see: C.Q. Jiao, C.A. DeJoseph, Jr., A. Garscadden, J. Chem. Phys., 117 (2002) 161 (and references therein).
[29] Y.K. Kim, M.E. Rudd, Phys. Rev. A 50 (1994) 3594.
[30] K. Irikura, NIST, Gaithersburg, MD, Private Communication.
[31] S.G. Lias, J.E. Bartmess, J.F. Liebman, J.L. Holmes, R.D. Levin, W.G. Mallard, J. Phys. Chem. Ref. Data 17 (1988).
[32] D.R. Lide (Ed.), CRC Handbook of Chemistry and Physics, 81st ed., CRC Press, Washington, DC, 2000.
[33] W.M.D. Bryant, J. Polym. Sci. 56 (1962) 277.
[34] B.S. Freiser, J.L. Beauchamp, J. Am. Chem. Soc. 96 (1974) 6260.
[35] H.M. Rosenstock, K. Draxl, B.W. Steiner, J.T. Herron, J. Phys. Land Chem. Ref. Data 6 (1977).
[36] I. Sauers, L.G. Christophorou, J.G. Carter, J. Chem. Phys. 71 (1979) 3016.
[37] D.H. Williams, I. Howe, Principles of Organic Mass Spectrometry, McGraw-Hill, London, 1972.
[38] R.C. Dunbar, Encyclopedia of Mass Spectrometry, Vol. 1, Theory and Ion Chemistry, edited by M.L. Gross, R. Caprioli, Volume Editor P.B. Armentrout, Elsevier, Inc., San Diego, 2003.
[39] T. Su, L. Kevan, J. Phys. Chem. 77 (1973) 148.
[40] R.A. Morris, A.A. Viggiano, J.F. Paulson, J. Phys. Chem. 97 (1993) 6208.